LETTER

Power-law partition and entropy production of high-energy cosmic rays: Knee-ankle structure of the all-particle spectrum

To cite this article: Roman Tomaschitz 2013 *EPL* **104** 19001

A Letters Journal Exploring the Frontiers of Physics

October 2013

EPL, **104** (2013) 19001 www.epljournal.org
doi: 10.1209/0295-5075/104/19001

Power-law partition and entropy production of high-energy cosmic rays: Knee-ankle structure of the all-particle spectrum

Roman Tomaschitz[(a)]

Department of Physics, Hiroshima University - 1-3-1 Kagami-yama, Higashi-Hiroshima 739-8526, Japan

received 31 July 2013; accepted in final form 3 October 2013
published online 4 November 2013

PACS 98.70.Sa – Cosmic rays (including sources, origin, acceleration, and interactions)
PACS 52.25.Kn – Thermodynamics of plasmas
PACS 95.30.Tg – Thermodynamic processes, conduction, convection, equations of state

Abstract – A statistical description of the all-particle cosmic-ray spectrum is given in the 10^{14} eV to 10^{20} eV interval. The high-energy cosmic-ray flux is modeled as an ultra-relativistic multi-component plasma, whose components constitute a mixture of nearly ideal but nonthermal gases of low density and high temperature. Each plasma component is described by an ultra-relativistic power-law density manifested as spectral peak in the wideband fit. The "knee" and "ankle" features of the high– and ultra-high–energy spectrum turn out to be the global and local extrema of the double-logarithmic E^3-scaled flux representation in which the spectral fit is performed. The all-particle spectrum is covered by recent data sets from several air shower arrays, and can be modeled as three-component plasma in the indicated energy range extending over six decades. The temperature, specific number density, internal energy and entropy of each plasma component are extracted from the partial fluxes in the broadband fit. The grand partition function and the extensive entropy functional of a non-equilibrated gas mixture with power-law components are derived in phase space by ensemble averaging.

Introduction. – The high– and ultra-high–energy cosmic-ray flux (10^{14}–10^{20} eV) [1] has been measured by air shower arrays such as Tibet-III [2], KASCADE [3], KASCADE-Grande [4], IceCube [5], HiRes-I and II [6], the Telescope Array [7,8] and the Pierre Auger Observatory [9], as well as by the HEGRA [10], AKENO [11], GAMMA [12], Yakutsk [13] and AGASA [14] arrays. Here, the goal is to give a statistical description of the broadband spectrum by means of classical ultra-relativistic power-law distributions. We fit the all-particle spectrum with the flux density of a dilute three-component plasma (non-equilibrated, with components at different temperature) and locate the "knees" and "ankles" [1,15–17] of the spectrum. The knees are identified as the peaks of the power-law distributions of the plasma components, and the ankles turn out to be the minima in the cross-over regimes of the partial fluxes. These extrema clearly emerge in the E^3-scaled flux representation employed in the wideband fit.

We sketch the basic thermodynamic formalism of classical ultra-relativistic power-law ensembles and nonthermal mixtures thereof, starting with the spectral number density parametrized with the Lorentz factor. We then define the specific number count and the internal energy of the gas components, as well as their entropy density. After this overview, we discuss the phase-space measure and probability density of nonthermal power-law ensembles, and derive the grand canonical partition function and the extensive entropy functional of multi-component power-law mixtures involving different particle species at different temperature.

We discuss the practical aspects of broadband spectral fitting with flux densities of classical unequilibrated (stationary non-equilibrium) power-law mixtures in the ultra-relativistic regime, and perform the spectral fit of the all-particle cosmic-ray spectrum above 10^{14} eV. The spectral flux density of a power-law distribution admits a power-law ascent linear in the log-log flux representation, and a curved descending power-law slope. The curvature is caused by the exponential cutoff determined by the temperature parameter of the Boltzmann factor [18,19]. The broadband spectrum of the all-particle mixture consists of overlapping spectral peaks generated by the partial fluxes of the individual plasma components. By choosing a

(a) E-mail: tom@geminga.org

suitable flux representation (double-logarithmic $E^3F(E)$), we find secondary knees and ankles in the all-particle spectrum. We calculate the thermodynamic parameters of each gas component, and estimate the entropy production of high-energy cosmic rays.

Mixtures of ultra-relativistic gases in stationary non-equilibrium. – An ultra-relativistic classical gas mixture composed of nonthermal power-law components is defined by the spectral number density

$$\begin{aligned} \mathrm{d}\rho_{\mathrm{mix}}(\gamma) &= \sum_{i=1}^{M} \mathrm{d}\rho_i(\gamma), \\ \mathrm{d}\rho_i(\gamma) &= \frac{m_i^3 s_i}{2\pi^2(\hbar c)^3} \frac{\mathrm{e}^{-\beta_i\gamma-\alpha_i}}{G_i(\gamma)} \sqrt{\gamma^2-1}\gamma\mathrm{d}\gamma, \end{aligned} \tag{1}$$

parametrized by the Lorentz factor γ. The positive spectral functions $G_i(\gamma)$ in the denominator of the power-law components $\mathrm{d}\rho_i(\gamma)$ are normalized as $G_i(1) = 1$ and are to be determined from a spectral fit. An M-component mixture is composed of particle species (Z_i, m_i), $i = 1, \ldots, M$, where m_i is the mass and Z_i the (positive or negative) integer charge number (in multiples of the electron charge $e > 0$) of the particles in the respective component (Z_i, m_i). The mass parameter m_i is a shortcut for m_ic^2, so that $E = m_i\gamma$ is the particle energy in an ideal gas mixture. s_i is the spin multiplicity and $\beta_i = m_i/(k_{\mathrm{B}}T_i)$ the dimensionless temperature parameter, with Boltzmann constant k_{B}. The mixture need not be equilibrated, admitting components at different temperature. The densities (1) are based on grand canonical partitions, allowing a fluctuating particle number via the dimensionless real fugacity parameter α_i, which is related to the chemical potential μ_i of each gas component by $\alpha_i = -\beta_i\mu_i/m_i$, and $z_i = \mathrm{e}^{-\alpha_i}$ is the fugacity. The ensemble average leading to (1) is discussed in the next section. The spectral function $G_i(\gamma)$ is a linear combination of two power laws,

$$G_i(\gamma) = \gamma^{\delta_i}\frac{g_i(\gamma)}{g_i(1)}, \quad g_i(\gamma) = 1 + a_i\gamma^{\sigma_i}, \tag{2}$$

where δ_i and σ_i are real power-law exponents and the amplitude a_i is positive. Spectral functions of this type are thermodynamically stable [18] and suitable to model wideband spectra [20–22]. Quantized power-law ensembles with $a_i = 0$ have been studied in [23,24].

The total particle number $N_{\mathrm{mix}} = \sum_{i=1}^{M} N_i$ and the internal energy $U_{\mathrm{mix}} = \sum_{i=1}^{M} U_i$ of a nonthermal gas mixture in a volume V are determined by the partial densities $\mathrm{d}\rho_i(\gamma)$ in (1),

$$N_i = V\int_{\gamma_i^{\mathrm{cut}}}^{\infty} \mathrm{d}\rho_i(\gamma), \qquad U_i = m_iV\int_{\gamma_i^{\mathrm{cut}}}^{\infty} \gamma\mathrm{d}\rho_i(\gamma). \tag{3}$$

The lower integration boundary is the cutoff Lorentz factor $\gamma_i^{\mathrm{cut}} \geq 1$, referring to particles of a given species (Z_i, m_i) with energies exceeding $E_i^{\mathrm{cut}} = m_i\gamma_i^{\mathrm{cut}}$, and adjusted to the energy range of the available data sets. The ultra-relativistic limit of the power-law densities $\mathrm{d}\rho_i(\gamma)$ is obtained by replacing $\sqrt{\gamma^2-1} \to \gamma$ in (1) and is applicable if $\gamma_i^{\mathrm{cut}} \gg 1$. The thermal relativistic Maxwell-Boltzmann distribution is recovered with $\delta_i = 0$, $g_i(\gamma) = 1$ and $\gamma_i^{\mathrm{cut}} = 1$ as lower integration boundary in (3).

The partition function of a gas component (Z_i, m_i) is denoted by $Z_{(Z_i,m_i)}$. Since particle number and internal energy are related to the grand partition function by $N_i = -(\log Z_{(Z_i,m_i)})_{,\alpha_i}$ and $U_i = -m_i(\log Z_{(Z_i,m_i)})_{,\beta_i}$, we can identify the partition function Z_{mix} of a nonthermal mixture as $\log Z_{\mathrm{mix}} = \sum_{i=1}^{M} \xi_i$, where $\xi_i = \log Z_{(Z_i,m_i)}$ and

$$\xi_i = V\frac{4\pi s_i m_i^3}{(2\pi\hbar c)^3}\mathrm{e}^{-\alpha_i}\int_{\gamma_i^{\mathrm{cut}}}^{\infty}\frac{\mathrm{e}^{-\beta_i\gamma}}{G_i(\gamma)}\sqrt{\gamma^2-1}\gamma\mathrm{d}\gamma. \tag{4}$$

Apparently $\xi_i = N_i$ holds for this classical distribution, and Z_{mix} is the product of the individual components $Z_{(Z_i,m_i)}$. Z_{mix} depends on the temperature variables β_i and the fugacity parameters α_i; the latter can be parametrized by particle number and temperature, $\alpha_i(\beta_i, N_i/V)$, by solving (4). The entropy of a nonthermal gas mixture is an extensive quantity,

$$S_{\mathrm{mix}} = \sum_{i=1}^{M} S_i, \quad S_i = k_{\mathrm{B}}\bigg(\log Z_{(Z_i,m_i)} + \frac{\beta_i}{m_i}U_i + \alpha_iN_i\bigg), \tag{5}$$

obtained from an ensemble average of power-law partitions, see the next section.

Power-law partitions of multi-component mixtures in phase space. – We give a probabilistic derivation of the classical spectral number density $\mathrm{d}\rho_{\mathrm{mix}}(\gamma)$ of an ultra-relativistic gas mixture in stationary non-equilibrium, cf. (1). To this end, we consider the phase space of n particles of a gas component (Z_i, m_i) labeled by charge number and mass in an M-component mixture, $i = 1, \ldots, M$. The phase-space measure of component (Z_i, m_i) is

$$\begin{aligned} \mathrm{d}^{3n}_{(Z_i,m_i)}(p,q) &= \frac{1}{(2\pi\hbar)^{3n}}\mathrm{d}^3p_1\mathrm{d}^3q_1\mathrm{d}^3p_2\mathrm{d}^3q_2\cdots\mathrm{d}^3p_n\mathrm{d}^3q_n, \\ \mathrm{d}^3p_k &= \frac{4\pi m_i^3}{c^3}\sqrt{\gamma_k^2-1}\gamma_k\mathrm{d}\gamma_k, \qquad k = 1, \ldots, n. \end{aligned} \tag{6}$$

The d^3q_k integrations range over a volume V, and the $\mathrm{d}\gamma_k$ integrations refer to the interval $\gamma_i^{\mathrm{cut}} \leq \gamma_k \leq \infty$, cf. after (3), where γ_i^{cut} is the cutoff Lorentz factor of the respective gas component (Z_i, m_i). The angular integration over the solid angle $\mathrm{d}\Omega$ has been carried out in (6) and gives the factor 4π. The scale factor $(2\pi\hbar)^{3n}$ renders the measure dimensionless.

Probability density and grand partition function of mixtures with power-law components. The probability density on the n-particle states of a gas component (Z_i, m_i)

factorizes as

$$f_n^{(Z_i,m_i)}(p,q) = \frac{s_i^n}{n!} b_n^{(Z_i,m_i)}(p,q) h_n^{(Z_i,m_i)}(p,q),$$
$$b_n^{(Z_i,m_i)} = \exp\Big(-\xi_i - \beta_i \sum_{k=1}^{n} \gamma_k - \alpha_i n \Big),$$
$$h_n^{(Z_i,m_i)} = \exp\Big(-\sum_{k=1}^{n} \log G_i(\gamma_k) \Big). \quad (7)$$

The factor $1/n!$ accounts for the indistinguishability within the particle species labeled (Z_i, m_i), and the positive integer s_i for the spin multiplicity of this component. $\beta_i = m_i/(k_\mathrm{B}T_i)$ is the temperature parameter of the respective gas component, and ξ_i is a normalization constant.

The normalization condition for the phase-space probability of an M-component mixture is

$$\int \sum_{n_1,\ldots,n_M=0}^{\infty} \prod_{i=1}^{M} f_{n_i}^{(Z_i,m_i)}(p,q) \mathrm{d}^{3n_i}_{(Z_i,m_i)}(p,q) = \prod_{i=1}^{M} \int \sum_{n=0}^{\infty} f_n^{(Z_i,m_i)}(p,q) \mathrm{d}^{3n}_{(Z_i,m_i)}(p,q) = 1, \quad (8)$$

where summation and integration sign can be interchanged, as well as the integration and product signs. The (p,q) variables of the density and measure will occasionally be omitted. The integrals in (8) factorize into one-particle states, and normalization is achieved by identifying $\xi_i = \log Z_{(Z_i,m_i)}$ in (7) with the partition function (4). Thus,

$$Z_{(Z_i,m_i)} = \sum_{n=0}^{\infty} \frac{s_i^n}{n!} \int \exp\left(-\beta_i \sum_{k=1}^{n} \gamma_k - \alpha_i n \right) h_n^{(Z_i,m_i)} \mathrm{d}^{3n}_{(Z_i,m_i)}, \quad (9)$$

for each gas component (Z_i, m_i). The partition function of an ideal mixture factorizes, $Z_\mathrm{mix} = \prod_{i=1}^{M} Z_{(Z_i,m_i)}$, or additively $\xi_\mathrm{mix} = \log Z_\mathrm{mix}$.

Entropy of a nonthermal gas mixture. The expectation values of particle number and internal energy of a gas component (Z_i, m_i) read

$$\sum_{n=0}^{\infty} \int n f_n^{(Z_i,m_i)}(p,q) \mathrm{d}^{3n}_{(Z_i,m_i)}(p,q) = -\frac{\mathrm{d}\xi_i}{\mathrm{d}\alpha_i} = \langle n \rangle_{(Z_i,m_i)} = N_i, \quad (10)$$

$$\sum_{n=0}^{\infty} \int \Big(m_i \sum_{k=1}^{n} \gamma_k \Big) f_n^{(Z_i,m_i)}(p,q) \mathrm{d}^{3n}_{(Z_i,m_i)}(p,q) = -m_i \frac{\mathrm{d}\xi_i}{\mathrm{d}\beta_i} = \langle u \rangle_{(Z_i,m_i)} = U_i, \quad (11)$$

where $u = m_i \sum_{k=1}^{n} \gamma_k$, and $N_i = \xi_i$, cf. (4). The spectral number density (1) follows from the phase-space average (10). The total particle count N_mix and internal energy U_mix are obtained by summing over the particle species, cf. (3). The total entropy $S_\mathrm{mix} = \sum_{i=1}^{M} S_i$ of the mixture is found by adding the partial entropies defined by the average

$$S_i = -k_\mathrm{B} \int \sum_{n=0}^{\infty} \frac{s_i^n}{n!} h_n^{(Z_i,m_i)} b_n^{(Z_i,m_i)} \log b_n^{(Z_i,m_i)} \mathrm{d}^{3n}_{(Z_i,m_i)}, \quad (12)$$

which is the expectation value $\langle s \rangle_{(Z_i,m_i)}$ of the phase-space random variable $s = k_\mathrm{B}(\xi_i + \beta_i \sum_{k=1}^{n} \gamma_k + \alpha_i n)$,

$$S_i = k_\mathrm{B} \int \sum_{n=0}^{\infty} \Big(\xi_i + \beta_i \sum_{k=1}^{n} \gamma_k + \alpha_i n \Big) f_n^{(Z_i,m_i)} \mathrm{d}^{3n}_{(Z_i,m_i)}. \quad (13)$$

The partial entropies S_i stated in (5) are recovered from (13) by substitution of the averages (10) and (11).

Spectral flux densities of nonthermal mixtures. – We write the components of the total spectral number density $\mathrm{d}\rho_\mathrm{mix}$ in (1) as

$$\frac{\mathrm{d}\rho_i(E)}{\mathrm{d}E} = 4\pi \frac{m_i^2 s_i \mathrm{e}^{-\alpha_i}}{(2\pi\hbar c)^3} \frac{g_i(1)}{g_i(\gamma)} \gamma^{1-\delta_i} \mathrm{e}^{-\beta_i \gamma} \sqrt{\gamma^2 - 1}, \quad (14)$$

with spectral function $g_i(\gamma)$ in (2), and replace the Lorentz factor by the particle energy $\gamma = E/m_i$. The mass m_i stands for $m_i c^2$, s_i is the spin degeneracy of component (Z_i, m_i), cf. after (1), and $z_i = \mathrm{e}^{-\alpha_i}$ the fugacity. $\beta_i = m_i/(k_\mathrm{B}T_i)$, and δ_i is a real power-law exponent. The amplitude of the second power law in $g_i(\gamma) = 1 + a_i \gamma^{\sigma_i}$ is positive, $a_i \geq 0$, and we will use positive exponents σ_i. Hence,

$$\frac{\mathrm{d}\rho_i(E)}{\mathrm{d}E} = \frac{4\pi s_i \mathrm{e}^{-\hat{\alpha}_i}}{(2\pi\hbar c)^3} \frac{E^{2-\delta_i} \mathrm{e}^{-\hat{\beta}_i E}}{1 + \hat{a}_i E^{\sigma_i}} \sqrt{1 - \frac{m_i^2}{E^2}}, \quad (15)$$

where we introduced the shortcuts $\hat{\beta}_i = 1/(k_\mathrm{B}T_i)$, $\hat{a}_i = a_i/m_i^{\sigma_i}$ and

$$\hat{\alpha}_i = \alpha_i - \log(1 + a_i) - \delta_i \log m_i. \quad (16)$$

We also note $\mathrm{e}^{-\hat{\alpha}_i} = z_i m_i^{\delta_i}(1 + a_i)$. We will use dimensionless quantities: E and m_i in eV units, and the units chosen for length, time and temperature are, respectively, meter, second and kelvin.

The spectral flux density of a gas component is found by multiplying the number density (15) with the particle velocity $\upsilon_i = c\sqrt{1 - m_i^2/E^2}$,

$$F_i(E) = \frac{c}{4\pi} \sqrt{1 - \frac{m_i^2}{E^2}} \frac{\mathrm{d}\rho_i}{\mathrm{d}E} = \frac{c s_i \mathrm{e}^{-\hat{\alpha}_i}}{(2\pi\hbar c)^3} \frac{E^{2-\delta_i} \mathrm{e}^{-\hat{\beta}_i E}}{1 + \hat{a}_i E^{\sigma_i}} \left(1 - \frac{m_i^2}{E^2} \right). \quad (17)$$

Density $F_i(E)$ is the number flux density per steradian; the energy flux is obtained by rescaling $F_i(E)$ with E.

Table 1: Thermodynamic parameters of the ultra-relativistic number densities $\mathrm{d}\rho_i/\mathrm{d}E$, cf. (15), generating the flux components $F_{i=1,2,3}(E)$ of the all-particle spectrum in fig. 1. N_i/V is the specific number density and U_i/V the energy density of the respective plasma component, calculated via (21) with lower cutoff energy $E_i^{\rm cut} \approx 10^{14}\,\mathrm{eV}$. Recorded are temperature T_i, fugacity z_i and chemical potential μ_i, cf. (20), as well as the partial entropy densities S_i/V, cf. (22). The fourth row lists the total specific densities $N_{\rm mix}/V$, $U_{\rm mix}/V$ and $S_{\rm mix}/V$ of the gas mixture, cf. (3) and (5). The entropy production is mainly due to the fugacity term in (22), and varies only weakly with particle mass, since the fugacities logarithmically enter the partial entropies. Fugacity, chemical potential and entropy are listed for a proton gas with $m_p \approx 938.27\times 10^6\,\mathrm{eV}$. Helium nuclei with mass $m_{\rm He}\approx 3.97m_p$ produce an entropy density of $S^{\rm He}_{\rm mix}/(k_{\rm B}V)\approx 3.8\times 10^{-10}$, and nickel nuclei with $m_{\rm Ni}\approx 58.7m_p$ produce $S^{\rm Ni}_{\rm mix}/(k_{\rm B}V)\approx 4.2\times 10^{-10}$, so that the actual mass composition, which is not yet known in the energy range of fig. 1, cannot significantly change the recorded protonic entropy estimates. At 10 GeV, the He/H abundance ratio is 0.048, and the Ni/H ratio is about 2×10^{-4} [17].

i	N_i/V [m^{-3}]	U_i/V [eV m^{-3}]	$k_{\rm B}T_i$ [eV]	$\log z_i$	μ_i [eV]	$S_i/(k_{\rm B}V)$ [m^{-3}]
1	3.15×10^{-12}	745	5×10^{18}	-113	-5.6×10^{20}	3.6×10^{-10}
2	1.25×10^{-14}	18	1.2×10^{19}	-131	-1.6×10^{21}	1.65×10^{-12}
3	6.6×10^{-18}	0.031	4.5×10^{20}	-136.5	-6.2×10^{22}	9.1×10^{-16}
mix	3.2×10^{-12}	763	–	–	–	3.6×10^{-10}

Wideband spectra are assembled by adding the partial flux densities of the gas components, $F_{\rm mix}(E)=\sum_{i=1}^{M}F_i(E)$. To locate the "knees" and "ankles" of the spectrum in log-log plots, it is convenient to rescale $F_{\rm mix}(E)$ with a suitable power E^k. The rescaled density $E^kF_{\rm mix}(E)$ is thus obtained by adding the partial fluxes

$$E^kF_i(E)[\mathrm{eV}^{k-1}\mathrm{m}^{-2}\mathrm{sr}^{-1}\mathrm{s}^{-1}]=\hat{y}_i\frac{E^{2+k-\delta_i}\mathrm{e}^{-\hat{\beta}_iE}}{1+\hat{a}_iE^{\sigma_i}}\left(1-\frac{m_i^2}{E^2}\right), \tag{18}$$

where we defined the amplitude

$$\hat{y}_i=\frac{cs_i\mathrm{e}^{-\hat{\alpha}_i}}{(2\pi\hbar c)^3}\approx 0.3146\times 10^{27}\frac{s_i}{2}\mathrm{e}^{-\hat{\alpha}_i}, \tag{19}$$

using dimensionless quantities, cf. after (16). In the ultra-relativistic regime, we can drop the factor $1-m_i^2/E^2$ in (18). Typically, the partial density (18) has a peak defined by an ascending power-law slope $E^{2+k-\delta_i}$ and a descending slope $E^{2+k-\delta_i-\sigma_i}$ terminating in exponential decay. The fitting parameters are the amplitudes $\hat{y}_i$, $\hat{a}_i$ and the exponents δ_i, σ_i determining location, height and the two power-law slopes of each peak, as well as the temperature parameter $\hat{\beta}_i$ defining the exponential cutoff.

The chemical potential $\mu_i=-\alpha_i/\hat{\beta}_i$, temperature and fugacity of each gas component can be extracted from the fitting parameters, cf. (16) and (19):

$$z_i=\frac{\mathrm{e}^{-\hat{\alpha}_i}}{m_i^{\delta_i}(1+\hat{a}_im_i^{\sigma_i})},\quad \mathrm{e}^{-\hat{\alpha}_i}\approx 3.18\times 10^{-27}\frac{2}{s_i}\hat{y}_i, \tag{20}$$

and $\mu_i[\mathrm{eV}]=k_{\rm B}T_i\log z_i$, with $k_{\rm B}T_i=1/\hat{\beta}_i$. All quantities are measured in units stated after (16). The specific particle density N_i/V in (3) reads

$$\frac{N_i}{V}[\mathrm{m}^{-3}]=\frac{4\pi}{c}\hat{y}_i\int_{E_i^{\rm cut}}^{\infty}\frac{E^{2-\delta_i}\mathrm{e}^{-\hat{\beta}_iE}}{1+\hat{a}_iE^{\sigma_i}}\sqrt{1-\frac{m_i^2}{E^2}}\mathrm{d}E, \tag{21}$$

where the lower energy cutoff (integration boundary) is related to the Lorentz factor by $E_i^{\rm cut}=m_i\gamma_i^{\rm cut}$. The energy density $U_i/V[\mathrm{eV}\ \mathrm{m}^{-3}]$, cf. (3), is obtained by adding a factor E to the integrand in (21). The specific densities N_i/V and U_i/V become independent of the particle mass m_i in the ultra-relativistic regime $m_i^2/E_i^{\rm cut2}\ll 1$, where the root in the integrand (21) can be dropped, so that the mass is absorbed in the fitting parameters. The partial entropies (5) are assembled from the specific number and energy densities,

$$\frac{1}{k_{\rm B}}\frac{S_i}{V}[\mathrm{m}^{-3}]=(1-\log z_i)\frac{N_i}{V}+\frac{1}{k_{\rm B}T_i}\frac{U_i}{V}, \tag{22}$$

where we have put $\alpha_i=-\log z_i$ in (5). Fugacity and temperature are extracted by way of (20). In the ultra-relativistic limit, we do not need to know the mass of the particles to calculate the specific number and energy densities (21) from the spectral fit. However, mass enters the entropy density through the fugacity, cf. table 1.

The multi-component plasma of high-energy cosmic rays. – The fit of the all-particle cosmic-ray spectrum in fig. 1 is performed with the ultra-relativistic limit of the flux density $F_{\rm mix}(E)$, cf. (18). We scale this density with E^3, defining $f_{\rm mix}=E^3F_{\rm mix}(E)$, so that

$$f_{\rm mix}(E)=\sum_{i=1}^{M}f_i,\qquad f_i(E)\sim\hat{y}_i\frac{E^{5-\delta_i}\mathrm{e}^{-\hat{\beta}_iE}}{1+\hat{a}_iE^{\sigma_i}}. \tag{23}$$

The fitting parameters in (23) are the power-law exponents δ_i, σ_i, the amplitudes $\hat{y}_i$, $\hat{a}_i$, and the temperature parameters $\hat{\beta}_i=1/(k_{\rm B}T_i)$ of the plasma components (Z_i,m_i), $i=1,\ldots,M$, cf. after (1). E is measured in eV units. The ultra-relativistic limit applies, since the fit is done above the cutoff energy $E_i^{\rm cut}\approx 10^{14}\,\mathrm{eV}$ where $m_i^2/E_i^{\rm cut2}\ll 1$, cf. the caption to table 1. In this limit, the mass-squares m_i^2 can be absorbed in the amplitudes $\hat{y}_i$, $\hat{a}_i$, cf. (16) and (19); the spin multiplicity is $s_i=2$.

The all-particle spectrum is fitted with three components, the flux densities $f_i=E^3F_i(E)$ generating the

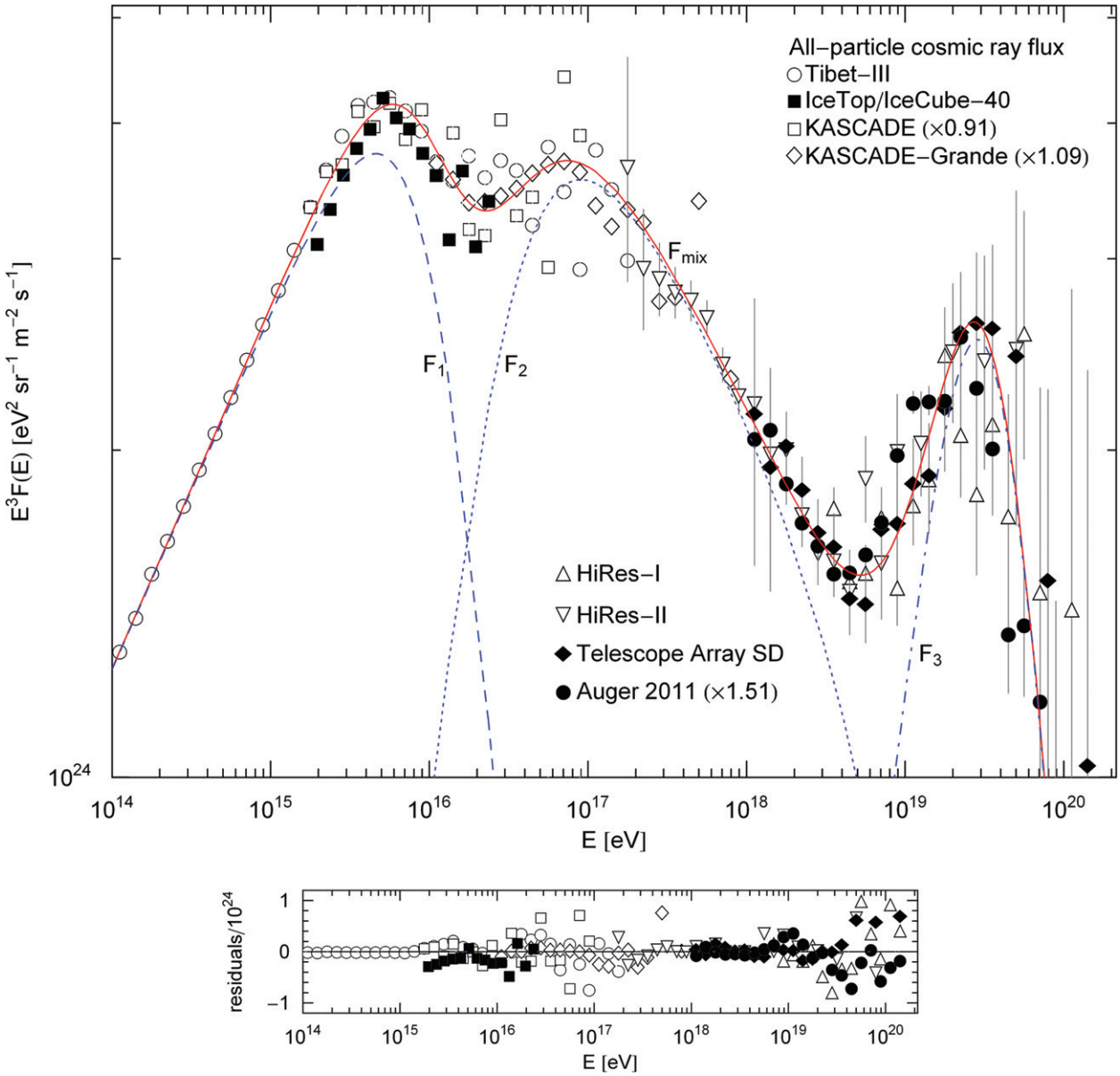

Fig. 1: (Colour on-line) All-particle cosmic-ray flux in the 10^{14}–10^{20} eV range. Data points from Tibet-III [2], IceTop/IceCube-40 [3], KASCADE [4], KASCADE-Grande [5], HiRes-I and HiRes-II [6], Telescope Array (Surface Detector) [7,8], and the Pierre Auger array [9]. The solid curve is a plot of the ultra-relativistic flux $F_{\rm mix}(E)$ (the total spectral number-flux density, scaled with E^3 in the figure) as stated in (23); the fitting parameters can be read off from the analytic representation of the flux components $f_i = E^3 F_i(E)$ in (24)–(26). The fit $F_{\rm mix}(E)$ is obtained by adding the partial fluxes $F_{i=1,2,3}(E)$ depicted as dashed and dotted peaks in the figure. The KASCADE, KASCADE-Grande and Auger data are rescaled to the Tibet-III data; the scale factors are indicated in the figure legend. The error bars of the data sets at lower energy are suppressed to avoid cluttering up the figure. The primary knee (maximum) of $F_{\rm mix}(E)$ is located at 6×10^{15} eV, a secondary ankle (minimum) at 2×10^{16} eV, a second knee at 7.5×10^{16} eV, the primary ankle at 5×10^{18} eV, and a third ultra-high–energy knee at about 3×10^{19} eV. The two ankles are the troughs in the cross-over regions of the partial fluxes, and the three knees are the spectral peaks. Each spectral component F_i has a power-law ascent linear in the log-log plot, followed by a descending power-law slope which is slightly bent because of the Boltzmann factor, cf. (23) and table 1.

overlapping peaks depicted in fig. 1:

$$f_1(E) = \frac{5.75 \times 10^{24} (E/\hat{E}_1)^{5-4.67}}{1 + 0.95 (E/\hat{E}_1)^{2.10}} \mathrm{e}^{-2\times 10^{-3}(E/\hat{E}_1)}, \quad (24)$$

$$f_2(E) = \frac{25 \times 10^{24} (E/\hat{E}_2)^{5-3.63}}{1 + 6.0 (E/\hat{E}_2)^{1.63}} \mathrm{e}^{-8.3\times 10^{-3}(E/\hat{E}_2)}, \quad (25)$$

$$f_3(E) = \frac{8.7 \times 10^{24} (E/\hat{E}_3)^{5-3.8}}{1 + 3.3 (E/\hat{E}_3)^{2.90}} \mathrm{e}^{-1.1\times 10^{-1}(E/\hat{E}_3)}, \quad (26)$$

where $\hat{E}_1 = 10^{16}$, $\hat{E}_2 = 10^{17}$ and $\hat{E}_3 = 5 \times 10^{19}$ are energy scales in eV, which are roughly determined by the location of the peaks, but otherwise arbitrarily chosen.

The introduction of an adaptable energy scale for each peak is useful in wideband fits, to keep the actual fitting parameters of each peak (the numerical constants in (24)–(26)) moderate or, in the case of the amplitudes, comparable. The fitting parameters (amplitudes $\hat{y}_i$, $\hat{a}_i$ and exponents δ_i, σ_i, $\hat{\beta}_i$, $i = 1, 2, 3$) can be read off from the partial densities (24)–(26) by comparison with (23), taking into account the numerical scaling factors $\hat{E}_i$. Once these parameters are determined, one can calculate the specific particle and internal energy densities $N_i/V[\mathrm{m}^{-3}]$ and $U_i/V[\mathrm{eV\ m}^{-3}]$ of the three plasma components via (21). The temperature of each component is obtained from $\hat{\beta}_i$, cf. after (20), the fugacity and chemical potential via (20), and the partial entropies via (22), cf. table 1.

Conclusion. – We have treated the all-particle spectrum of cosmic rays above an energy threshold of $10^{14}\,\mathrm{eV}$ as dilute multi-component plasma at high temperature. The statistical description given here does not involve any hypothetical assumptions on cosmological source or cut-off mechanisms. The contribution of the Coulomb interaction [25,26] to the partition function is negligible, since $e^2/(4\pi r k_{\mathrm{B}} T_i) \ll 1$, with interparticle distance $r = (N_{\mathrm{mix}}/V)^{-1/3}$ and fine-structure constant $e^2/(4\pi\hbar c) \approx 1/137$. (Temperature and specific particle density of each component are listed in table 1.) High-energy cosmic rays can thus be considered as ideal gas mixture, unequilibrated though, because of the power-law factors in the distribution functions and the different temperatures of the partial densities (1). Ultra-relativistic power-law partitions admit an extensive and stable entropy functional [18], based on a grand canonical phase-space average, and this also holds true for non-equilibrated ideal mixtures, as the partition function factorizes, cf. (9).

The three flux components of the all-particle spectrum depicted in fig. 1 differ in size but not structurally. Each of the partial fluxes admits an ascending power-law slope and a slightly curved decaying slope due to the exponential cutoff in the spectral number density. The power-law exponents and the temperature parameters of the three spectral components constituting the high-energy wideband are quite comparable, cf. (24)–(26). The descending slope of the third ultra-high–energy peak is not yet well determined by the presently available data points, as illustrated by the large spread of the residuals in this region, and a fourth peak above $10^{20}\,\mathrm{eV}$ is possible [1,14].

The spectral power-law densities (15) of the three plasma components have been empirically determined from the spectral fit in fig. 1, cf. (24)–(26), and the thermodynamic parameters are listed in table 1. In the scaled flux representation $E^3F(E)$ employed in the broadband fit, the primary knee of the all-particle spectrum at $6 \times 10^{15}\,\mathrm{eV}$ and the ankle at $5 \times 10^{18}\,\mathrm{eV}$ are the global extrema of the flux density. We have identified two secondary knees as local maxima generated by the spectral peaks of the partial fluxes, and one secondary ankle as local minimum in the cross-over region between the first and second peak, cf. the caption to fig. 1.

REFERENCES

[1] Nagano M., *New J. Phys.*, **11** (2009) 065012.
[2] Amenomori M. *et al.*, *Astrophys. J.*, **678** (2008) 1165.
[3] IceCube Collaboration (Abbasi R. *et al.*), *Astropart. Phys.*, **42** (2013) 15.
[4] Antoni T. *et al.*, *Astropart. Phys.*, **24** (2005) 1.
[5] Apel W. D. *et al.*, *Astropart. Phys.*, **36** (2012) 183.
[6] Abbasi R. U. *et al.*, *Phys. Rev. Lett.*, **100** (2008) 101101.
[7] Tsunesada Y. *et al.*, in *32nd International Cosmic Ray Conference, Beijing, China, 2011*, arXiv:1111.2507.
[8] Abu-Zayyad T. *et al.*, *Astrophys. J.*, **768** (2013) L1.
[9] Pierre Auger Collaboration (Abreu P. *et al.*), in *32nd International Cosmic Ray Conference, Beijing, China, 2011*, arXiv:1107.4809.
[10] Arqueros F. *et al.*, *Astron. Astrophys.*, **359** (2000) 682.
[11] Nagano M. *et al.*, *J. Phys. G*, **18** (1992) 423.
[12] Garyaka A. P. *et al.*, *J. Phys. G*, **35** (2008) 115201.
[13] Ivanov A. A. *et al.*, *New J. Phys.*, **11** (2009) 065008.
[14] Takeda M. *et al.*, *Astropart. Phys.*, **19** (2003) 447.
[15] Nagano M. and Watson A. A., *Rev. Mod. Phys.*, **72** (2000) 689.
[16] Aharonian F. *et al.*, *Space Sci. Rev.*, **166** (2012) 97.
[17] Nakamura K. *et al.*, *J. Phys. G*, **37** (2010) 075021.
[18] Tomaschitz R., *Physica A*, **385** (2007) 558.
[19] Tomaschitz R., *EPL*, **89** (2010) 39002.
[20] Band D. *et al.*, *Astrophys. J.*, **413** (1993) 281.
[21] Preece R. D. *et al.*, *Astrophys. J. Suppl. Ser.*, **126** (2000) 19.
[22] Lloyd N. M. and Petrosian V., *Astrophys. J.*, **543** (2000) 722.
[23] Tomaschitz R., *Physica A*, **387** (2008) 3480.
[24] Tomaschitz R., *Physica B*, **405** (2010) 1022.
[25] Ichimaru S., *Rev. Mod. Phys.*, **54** (1982) 1017.
[26] Ichimaru S., Iyetomi H. and Tanaka S., *Phys. Rep.*, **149** (1987) 91.